IEEE Open Journal of
Power Electronics

Received 2 May 2024; revised 29 May 2024; accepted 10 June 2024. Date of publication 13 June 2024;
date of current version 20 June 2024. The review of this article was arranged by Associate Editor Ui-Min Choi.

Digital Object Identifier 10.1109/OJPEL.2024.3414172

Coupling-Independent Capacitive Wireless Power Transfer With One Transmitter and Multiple Receivers Using Frequency Bifurcation

ARIS VAN IEPEREN [1] (Student Member, IEEE), STIJN DERAMMELAERE [1,2] (Member, IEEE), AND BEN MINNAERT [1] (Member, IEEE)

[1]CoSysLab, University of Antwerp, 2020 Antwerpen, Belgium
[2]AnSyMo/CoSys, Flanders Make, 3920 Lommel, Belgium

CORRESPONDING AUTHOR: ARIS VAN IEPEREN (e-mail: aris.vanieperen@uantwerpen.be.)

This work was supported by the Research Foundation Flanders (FWO) under Grant 1SH1224N.

ABSTRACT Capacitive wireless power transfer utilizes capacitive coupling to transfer electrical energy wirelessly. Due to the nature of the coupling, it is seen as a well-suited technique for single input multiple outputs configurations. For these systems, optimal solutions for power transfer and efficiency exist, however, with variation in distance or alignment, the coupling varies and as a result, these optimal solutions vary. Therefore, there is a need for coupling-independent approaches to keep these systems within their optimal operating conditions. In this work, we propose a frequency-agile mode, using frequency bifurcation, that allows for a nearly coupling-independent power transfer and efficiency regime for a capacitive wireless power transfer system with one transmitter and multiple receivers. The conditions for bifurcation are described and analytical expressions for the power and transducer gains are determined. It is shown that, when operating at the secondary resonances, nearly constant efficiency and power transfer to the load can be achieved. An experimental setup was realized and the results validate the theoretical results, showcasing a coupling-independent efficiency and power output with a more than four-fold increase in output power at the cost of less than 5% reduction in absolute efficiency.

INDEX TERMS Capacitive wireless power transfer, frequency bifurcation, single input multiple outputs.

I. INTRODUCTION

Capacitive wireless power transfer (CPT) is a form of near-field wireless power transfer (WPT) that utilizes capacitive coupling to transfer electrical energy between one or more transmitters to one or more receivers without the need for physical connections [1], [2], [3]. CPT offers several advantages, including flexibility in design, high efficiency, multi-device charging, environmental compatibility, and scalability, making it a promising technology for WPT in various applications, such as charging mobile devices, powering sensors in remote locations, and energizing implantable medical devices [4], [5], [6], [7].

As mentioned above, one of the advantages of CPT is multi-device charging, which refers to the ability of CPT to simultaneously charge or power multiple devices from a single transmitter, commonly referred to as a single input multiple outputs (SIMO) configuration. This can be particularly beneficial in scenarios where several devices must be charged at the same time, such as in smart homes, offices, or (public) vehicle charging stations [8], [9], [10].

For a given WPT system, it is known that an optimal output impedance exists for either maximizing power output or efficiency. However, with variation in distance or alignment the capacitive coupling changes, and as a result, this optimal output impedance changes [11], [12], [13]. Under varying coupling, such systems are either optimal coupled, over-coupled or under-coupled. It has been shown that in

the case of over-coupling, the power delivered at the load decreases [14].

Imposing a fixed coupling restriction for WPT systems is undesired, as this will constrain the flexibility since strict spacial alignment will be needed. Furthermore, a fixed coupling is not possible in dynamic environments, where a moving object is charged, such as for instance a driving car, which inevitably involves changes in coupling over time.

Therefore, solutions to maintain the optimum conditions under varying coupling are needed. Changing the value of the load is such a possibility, and this approach has the advantage that the operating frequency can be kept constant. However, this is not feasible for applications where the load is fixed.

Alternatively, a frequency-agile approach can sustain optimal conditions at fluctuating coupling for a fixed load value, by adjusting the operating frequency according to the coupling between the transmitter and receiver. Such design can be realized by applying frequency bifurcation, which is an interesting phenomenon observed in near-field WPT, where multiple frequencies exist for which the input impedance is matched (i.e., the input reactance equals zero), and hence, multiple resonant frequencies exist. Due to several challenges, including the limitations of variable frequency controllers in handling uncertainty within the bifurcation region, this frequency bifurcation is often undesired, and design rules are found to evade this phenomenon in WPT systems [15], [16], [17], [18]. However, frequency bifurcation can also be deliberately used in WPT systems, and special characteristics of the frequency bifurcation can be exploited for instance in foreign object detection [19].

Next to frequency bifurcation, a phenomenon called frequency splitting can occur in WPT systems, where multiple resonant peaks exist at the load of the receiver [20], [21], [22]. Although both phenomena relate to changes in resonance frequencies, notable differences exist. While frequency bifurcation concerns the input characteristics, with the characteristic equation given by:

$$\mathrm{Im}(Z_{in}) = 0, \tag{1}$$

where Z_{in} is the input impedance, frequency splitting is focused on the output features of the WPT systems, with the characteristic equation given by:

$$\frac{\partial P_L}{\partial \omega} = 0, \tag{2}$$

where P_L is the load power and ω the operating frequency. Both phenomena occur at a specific value of the coupling coefficient k, denoted as k_b and k_{split} for bifurcation and splitting frequencies, respectively. Typically, the values of k_b and k_{split} differ [22], underscoring their unique nature within the system.

In [14], a (nearly) constant efficiency and power transfer is realized by applying frequency bifurcation to single input single output (SISO) inductive wireless power transfer (IPT) systems. The secondary resonant frequencies are derived, and analytical results are presented. Similarly, in [23], frequency bifurcation is applied to SISO CPT systems, and expressions for the power gain G_P and transducer gain G_T are derived, which are shown to be independent of the coupling coefficient for the secondary resonances. The results are validated by circuit simulation. In this paper, we derive expressions for the power gain G_P and transducer gain G_T for SIMO CPT systems, for any number of receivers, and we show that they are coupling-independent which we proof by circuit simulation and experimental data.

Besides frequency bifurcation, other approaches of frequency tuning to achieve coupling-independent WPT have been explored in the literature. In [24], a frequency tuning method utilizing the reflection coefficient is proposed for a WPT system, and it is demonstrated to have better performance in terms of power and efficiency compared to using the zero phase angle method. However, a SISO IPT system is used, in contrast to our SIMO CPT system. In [25], a CPT system that leverages Parity-Time symmetry to maintain constant output power is presented. This is achieved by configuring the input power supply as a negative resistor through a phase difference of 180 ° between the input voltage and current. This approach ensures constant output power and stable transfer efficiency even with significant coupler misalignment. However, the system in this study is also a SISO configuration, whereas our system features a SIMO CPT design. The work presented in [26] discusses a 10 MHz CPT system with multiple outputs. Despite its capability to maintain a constant output voltage across multiple outputs, this system does not guarantee constant power and efficiency. In contrast, our system offers the advantage of constant power and efficiency across multiple outputs, providing a more robust solution for practical applications in multi-output CPT systems. The comparison between the proposed CPT system with existing literature is summarized in Table 1.

The conditions for frequency bifurcation in SIMO CPT systems have been derived in [27], however, the analytical derivation was restricted to a system with two receivers. In this work, we extend the derivation of the conditions towards systems with any number of receivers. Furthermore, to the best of our knowledge, a coupling-independent solution for SIMO CPT has not been presented in analytic form, and literature lacks experimental results in this regard. Hence, the coupling-independent regime, originated by the bifurcation phenomenon has not been explored for these SIMO systems yet.

In this study, we will investigate the application of a frequency-agile approach utilizing the bifurcation phenomenon to achieve a CPT system with one transmitter and multiple receivers which efficiency and power transfer remain unaffected by fluctuations of the coupling. The system and a mathematical notation using the admittance matrix are presented, and the input admittance is used to determine the conditions for bifurcation. Analytical expressions for the power and transducer gains are derived, and, using the bifurcation conditions, expressed in normalized circuit parameters. The results are visually presented, showing a nearly constant

TABLE 1. Comparison Between the Proposed CPT System and the Existing Literature

Reference	IPT/CPT	Method	Multiple ouputs	Coupling-independent power and efficiency	Experimental data
[14]	IPT	Bifuration	No	Yes	No
[23]	CPT	Bifurcation	No	Yes	No
[24]	IPT	Reflection coefficient	No	Yes	Yes
[25]	CPT	Parity-Time symmetry	No	Yes	Yes
[26]	CPT	LCCL compensation	Yes	No	Yes
This work	CPT	Bifurcation	Yes	Yes	Yes

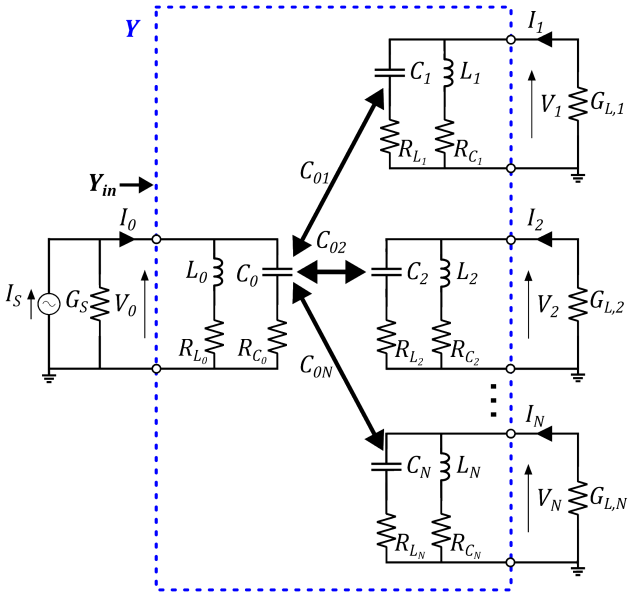

FIGURE 1. Equivalent circuit representation of a single input, multiple outputs CPT system.

efficiency and power transfer regime with significantly increased output power compared to a fixed frequency approach.

In [28] we presented a coupling-independent solution for a CPT system with one transmitter and two receivers in analytic form, and explored the, by the bifurcation phenomenon originated, coupling-independent efficiency and power transfer regime. In this work, we extend the theoretical derivation to N receivers and validate our results using an experimental setup with one transmitter and two receivers, confirming the theoretical results. To the best of our knowledge, this is the first time that a coupling-independent regime with multiple receivers has been both analytically and experimentally demonstrated for a capacitive wireless power transfer system.

II. METHODS

A. CIRCUIT DESCRIPTION

We consider the equivalent circuit of a CPT system with a single transmitter and multiple receivers [27], ignoring the cross-coupling between the individual receivers which are typically small compared to the coupling between the transmitter and receivers, as shown in Fig. 1. The supply of the transmitter is represented by a sinusoidal current source with an angular operating frequency ω_0 and peak value I_S, and shunt conductance G_S. The purely resistive load of the receivers is given by conductances $G_{L,k}$ $(k = 1, 2, .., N)$. The capacitive link is represented by the capacitances C_i $(i = 0, 1, .., N)$, and their mutual coupling capacitances C_{0k}. The shunt inductances L_i, with an inductance of $1/\omega_0^2 C_i$, are used to create a resonant circuit. The inductor and capacitor losses are taken into account by their equivalent series resistances (ESRs), R_{L_i} and R_{C_i}. Note that because of the introduction of these ESRs, the resonant frequency is slightly changed, however, this change is small for practical CPT systems and can therefore be neglected [23].

B. ADMITTANCE MATRIX

The CPT system can be considered as a multiport with one input port and N output ports, indicated in Fig. 1, which can be represented by an admittance matrix $\mathbf{Y}$ [29]:

$$\mathbf{Y} = \begin{bmatrix} y_{00} & y_{01} & \cdots & y_{0N} \\ y_{10} & y_{11} & \cdots & y_{1N} \\ \vdots & \vdots & \ddots & \vdots \\ y_{N0} & y_{N1} & \cdots & y_{NN} \end{bmatrix}. \tag{3}$$

The diagonal and off-diagonal terms of the admittance matrix $\mathbf{Y}$ are given by:

$$y_{xx} = \frac{1}{R_{L_x} + j\omega L_x} + \frac{1}{R_{C_x} + \frac{1}{j\omega C_x}}, \tag{4}$$

$$y_{xy} = -j\omega C_{xy}. \tag{5}$$

In order to generalize the circuit analysis, for any possible operating frequency and power levels, it is convenient to introduce normalized quantities. We define the normalized frequency u as:

$$u = \frac{\omega}{\omega_0}, \tag{6}$$

and the normalized ESRs and load conductances r_{C_i}, r_{L_i} and $g_{L,k}$ as:

$$r_{C_i} = \omega_0 C_i R_{C_i}, \tag{7}$$

$$r_{L_i} = \frac{R_{L_i}}{\omega_0 L_i}, \tag{8}$$

$$g_{L,k} = \frac{G_{L,k}}{\omega_0 C_k}. \tag{9}$$

Note that these normalized values represent the reciprocal of the quality factor ($1/Q$) of the individual components.

For high-quality factors (i.e., efficient passive components), commonly encountered in practical CPT applications, we can simplify the admittance matrix with the normalized quantities by neglecting the squared normalized resistances with respect to u^2, and find the diagonal and off-diagonal entries of the approximate admittance matrix $\mathbf{Y_a}$ as [23]:

$$y_{xx} = \omega_0 C_x \left(r_{C_x} u^2 + \frac{r_{L_x}}{u^2} + j\frac{u^2-1}{u} \right), \tag{10}$$

$$y_{xy} = -j\sqrt{C_x C_y}\,\omega_0 k_{xy} u, \tag{11}$$

with k_{xy} the coupling coefficient, given by:

$$k_{xy} = \frac{C_{xy}}{\sqrt{C_x C_y}}. \tag{12}$$

C. INPUT ADMITTANCE

The input admittance Y_{in} of the considered multiport system is given by [30]:

$$Y_{in} = y_{00} + \frac{1}{M_{00}} \sum_{j=1}^{N} (-1^j) y_{0j} M_{0j}, \tag{13}$$

with M_{0i} the minor of the matrix $\mathbf{Y_a} + \mathbf{Y_L}$ and $\mathbf{Y_L}$ the diagonal load admittance matrix.

To simplify the notation, the following definitions are introduced:

$$a_k = 1 + 2 g_{L,k} r_{C_k} \tag{14}$$

$$b_k = 2 - g_{L,k}^2 \tag{15}$$

$$c_k = 1 + 2 g_{L,k} r_{L_k} \tag{16}$$

$$d = \sum_{j=0}^{N} r_{L_j} \tag{17}$$

$$e = \sum_{j=0}^{N} r_{C_j} \tag{18}$$

$$r_i = r_{L_i} + r_{C_i}. \tag{19}$$

We can express the real (g_{in}) and imaginary (b_{in}) parts of the normalized input admittance $y_{in} = Y_{in}/\omega_0 C_0$ by neglecting $r_{C_i}^2$, $r_{L_i}^2$ and $r_{C_i} r_{L_i}$ with respect to u^2 as:

$$g_{in} = r_{C0} u^2 + \frac{r_{L0}}{u^2} + \sum_{j=1}^{N} \frac{k_{0j}^2\, u^2 \left(r_{Cj} u^4 + g_{Lj} u^2 + r_{Lj} \right)}{a_j u^4 - b_j u^2 + c_j}, \tag{20}$$

$$b_{in} = \frac{u^2-1}{u} \left(1 - \sum_{j=1}^{N} \frac{k_{0j}^2\, u^4}{a_j u^4 - b_j u^2 + c_j} \right). \tag{21}$$

From (21) it is evident that the input susceptance b_{in} equals zero if the normalized frequency u is one, i.e., at the resonant frequency ω_0. We call this the primary resonant frequency. Furthermore, it is apparent that other frequencies exist where the input susceptance equals zero. We can find these other frequencies by substituting $u^2 = x$, and solving the quartic equation:

$$\sum_{j=1}^{N} \frac{k_{0j}^2 x^2}{a_j x^2 - b_j x + c_j} = 1. \tag{22}$$

For a system with identical receivers (i.e., $a_j = a$, $b_j = b$ and $c_j = c$, $\forall j$), this quartic equation reduces to:

$$\left(a - k_{sum}^2\right) x^2 - bx + c = 0, \tag{23}$$

with k_{sum}^2 equal to:

$$k_{sum}^2 = \sum_{j=1}^{N} k_{0j}^2. \tag{24}$$

For a CPT system that fulfills the requirement of a non-negative discriminant (i.e. $\sum_{j=1}^{N} k_{0j}^2 < a - \frac{b^2}{4c}$) and $\sum_{j=1}^{N} k_{0j}^2 < a$, only the primary resonant frequency is present for $b < 0$, and two distinct secondary frequencies exist for $b > 0$, following [27]:

$$u_{\pm} = \sqrt{\frac{b \pm \sqrt{b^2 - 4c\left(a - k_{sum}^2\right)}}{2\left(a - k_{sum}^2\right)}}. \tag{25}$$

At the primary ($u = 1$) and secondary ($u = u_{\pm}$) resonant frequencies, the normalized input admittance is real and equals:

$$g_{in}(u=1) = r_0 + \sum_{j=1}^{N} \frac{\left(g_{L,j} + r_j\right) {k_{0j}}^2}{a_j - b_j + c_j}, \tag{26}$$

$$g_{in}(u=u_{\pm}) = g_L + \frac{bd}{c} + \frac{1}{2}\left(\frac{e}{a - k_{sum}^2} - \frac{d}{c} \right) h_{\pm}, \tag{27}$$

with $h_{\pm}$ equal to:

$$h_{\pm} = \left(b \pm \sqrt{b^2 - 4c\left(a - k_{sum}^2\right)} \right). \tag{28}$$

D. POWER GAIN

The power gain G_P, commonly referred to as the efficiency of a WPT network, is defined as the ratio of the load power P_L, which is the sum of the power of each individual load, to the input power P_{in}. For the given WPT system, the input power is given by:

$$P_{in} = \frac{1}{2} G_{in} |V_0|^2 \tag{29}$$

and the total power dissipated at the loads is given by:

$$P_L = \frac{1}{2} \sum_{j=1}^{N} G_{L,j} |V_j|^2, \tag{30}$$

which gives us the following expression for the power gain:

$$G_P = \frac{P_L}{P_{in}} = \sum_{j=1}^{N} \frac{G_{L,j}}{G_{in}} \left|\frac{V_j}{V_0}\right|^2. \tag{31}$$

We can express $\frac{V_j}{V_0}$ as a function of the system admittances as:

$$\frac{V_j}{V_0} = \frac{-y_{j0}}{y_{jj} + Y_{L,j}}, \tag{32}$$

with $Y_{L,j}$ the load admittances.

Using a simple but elaborate algebraic restatement, we can express (31) as:

$$G_P = \sum_{j=1}^{N} \frac{k_{0j}^2\, u^4}{a_j u^4 - b_j u^2 + c_j} \frac{g_{L,j}}{g_{in}}. \tag{33}$$

For a system with identical receivers (33) simplifies to:

$$G_P = \frac{k_{sum}^2\, u^4}{a u^4 - b u^2 + c} \frac{g_L}{g_{in}}, \tag{34}$$

with $g_L = \sum_{j=1}^{N} g_{L,j}$. At the primary and secondary resonant frequencies, the power gain is given by:

$$G_P(u=1) = \frac{k_{sum}^2 g_L}{g_L r_0 (g_L + 2r_1) + k_{sum}^2 (g_L + r_1)}, \tag{35}$$

$$G_P(u=u_\pm) = \frac{g_L}{g_L + \frac{bd}{c} + \frac{1}{2}\left(\frac{e}{a - k_{sum}^2} - \frac{d}{c}\right) h_\pm}. \tag{36}$$

E. TRANSDUCER GAIN

The transducer gain G_T is defined as the ratio of the load power P_L to the available power of the generator, P_{AG}. For a fixed P_{AG}, maximizing G_T corresponds to maximizing the amount of power transfer to the load.

For the given CPT system, the available power of the generator is given by:

$$P_{AG} = \frac{|I_s|^2}{8 G_S}, \tag{37}$$

which results into the following expression for the transducer gain:

$$G_T = \frac{P_L}{P_{AG}} = \sum_{j=1}^{N} \frac{4 G_S G_{L,j} |V_j|^2}{|I_S|^2} \tag{38}$$

We can express V_j as a function of the system admittances and peak value of the current source I_S by multiplying (32) with V_0, where V_0 is given by:

$$V_0 = \frac{I_S}{Y_S + y_{00} - \sum_{j=1}^{N} \frac{y_{0j} y_{j0}}{y_{jj} + Y_{L,j}}}. \tag{39}$$

Using a simple but elaborate algebraic restatement, we can express (38) as:

$$G_T = \frac{4 g_{in} g_S}{|y_{in} + g_S|^2} G_p. \tag{40}$$

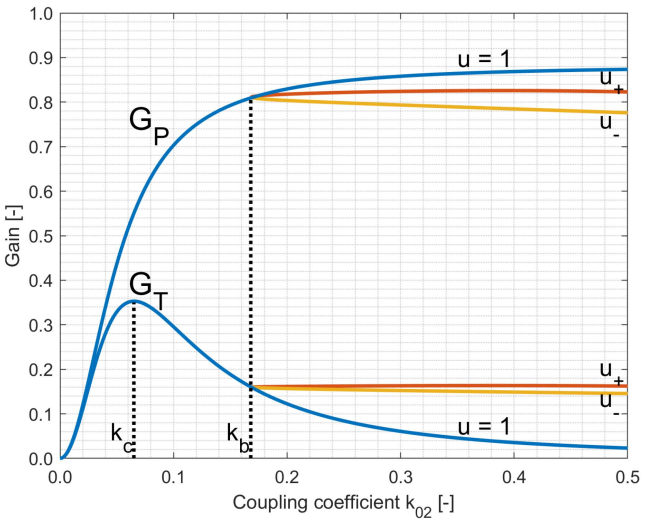

FIGURE 2. Power gain G_P and transducer gain G_T, as a function of the coupling coefficient k_{02}, with the critical coupling k_c and bifurcation coupling k_b indicated, for a coupling coefficient k_{01} equal to zero.

At the primary and secondary resonant frequencies, the transducer gain is given by:

$$G_T(u=1) = \frac{4 k_{sum}^2 g_S g_L^2 (g_L + 2r_1)}{\left[k_{sum}^2 (g_L + r_1) + g_L (g_S + r_0)(g_L + 2r_1)\right]^2} \tag{41}$$

$$G_T(u=u_\pm) = \frac{4 g_S g_L}{\left[g_S + g_L + \frac{bd}{c} + \frac{1}{2}\left(\frac{e}{a - k_{sum}^2} - \frac{d}{c}\right) h_\pm\right]^2}. \tag{42}$$

It is worth mentioning that in the lossless case ($r_{C_i} = 0$, $r_{L_i} = 0$), the denominators of (36) and (42) reduce to g_L and $(g_S + g_L)^2$ respectively, and hence, at the secondary resonances, the gains are independent of k_{xy}. Furthermore, high inductor and capacitor quality factors will give relatively low values for r_{C_i} and r_{L_i}, which result in the parameters d and e, present in all coupling-dependent terms in (36) and (42), being small with respect to g_L. Therefore, nearly coupling-independent gains can be achieved.

III. RESULTS AND DISCUSSION

A. THEORETICAL RESULTS

We consider a CPT system with one transmitter and two identical receivers, with $g_S = r_{L_0} = 0.010$, $r_{L_1} = r_{L_2} = 0.015$, $r_{C_0} = r_{C_1} = r_{C_2} = 0.005$ and $g_{L,1} = g_{L,2} = 0.150$. The quantities are chosen such that they align with those utilized in previously published works, which allows for validation of our results with existing research [23], [27]. The presented approach is applicable to systems with non-identical receivers as well, results regarding these systems can be found in [28].

Figs. 2 and 3 show the power gain G_P and the transducer gain G_T as a function of the coupling coefficient k_{02} for a coupling coefficient k_{01} equal to zero and 0.1 respectively.

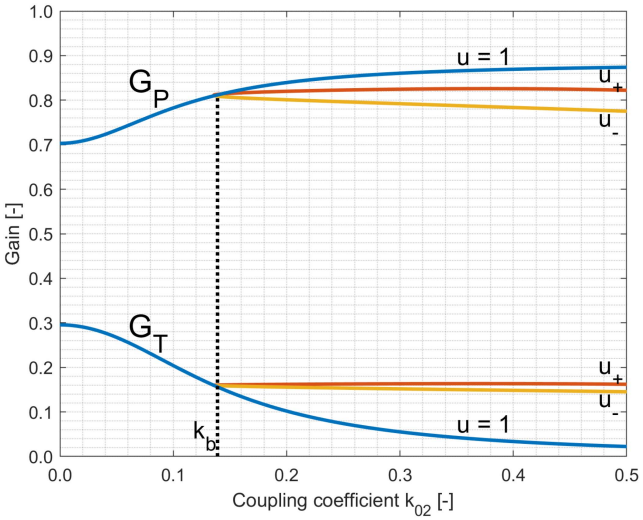

FIGURE 3. Power gain G_P and transducer gain G_T, as a function of the coupling coefficient k_{02}, with the bifurcation coupling k_b indicated, for a coupling coefficient k_{01} equal to 0.1.

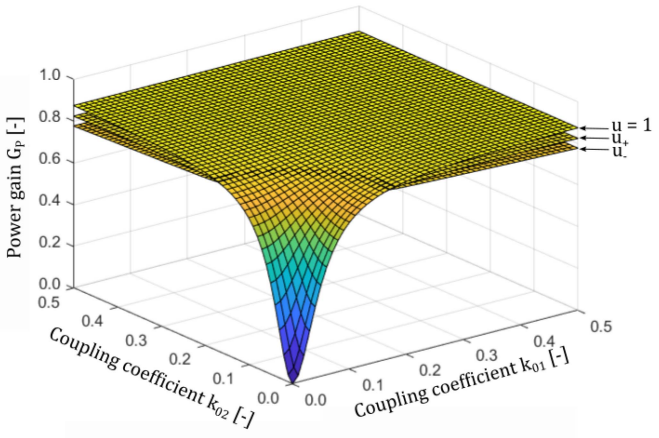

FIGURE 4. Power gain G_P as a function of the coupling coefficients k_{01} and k_{02} for a system with two equal receivers.

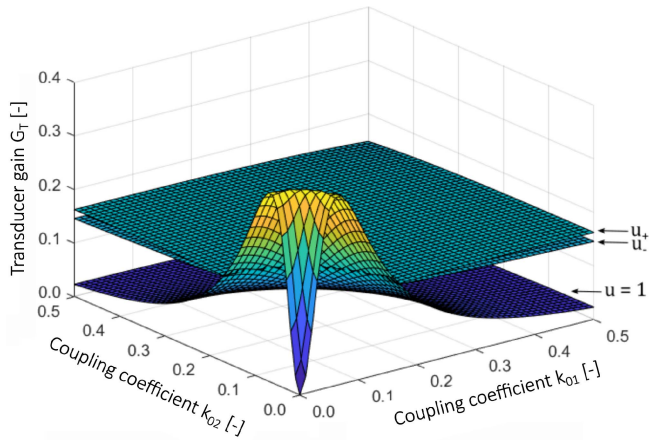

FIGURE 5. Transducer gain G_T as a function of the coupling coefficients k_{01} and k_{02} for a system with two equal receivers.

Note that k_{01} equal to zero corresponds with a system that only has one receiver (i.e., a SISO system), and the result matches [23].

In both scenarios, at the primary resonance ($u = 1$), the power gain G_P increases with an increasing coupling coefficient k_{02}. For k_{01} equal to zero, the transducer gain G_T increases with an increasing coupling coefficient k for a coupling below the optimal coupling coefficient k_c (i.e., the coupling coefficient that maximizes the power transfer), and decreases again for a coupling coefficient larger than the optimal coupling coefficient. As k_{01} equal to 0.1 is already larger than k_c, the maximum G_T is found at k_{02} equal to zero and decreases with increasing k_{02}.

For a coupling coefficient higher than the bifurcation coupling k_b (i.e. the minimum coupling coefficient that fulfills the bifurcation requirement), the secondary resonances $u_\pm$ are shown. In both scenarios, G_P and G_T increase slightly for u_+ and decrease slightly for u_-. We can clearly see the advantage of the coupling-independent modes for CPT applications: we obtain a higher power transfer to the load at the expense of only a small reduction in efficiency.

Fig. 4 shows the power gain G_P as a function of the coupling coefficients k_{01} and k_{02} for the given system. For the primary resonance, G_P increases for higher coupling coefficients. For the secondary resonances $u_\pm$, a nearly constant G_P can be observed for varying coupling, indicating the nearly coupling-independent efficiency. Note that the side along the k_{02} axis corresponds to Fig. 2.

Fig. 5 shows the transducer gain G_T as a function of the coupling coefficients k_{01} and k_{02} for the given system. G_T increases with the coupling coefficients until the sum of the coupling coefficients reaches the optimal coupling coefficient. For coupling coefficients $k_{01} + k_{02} > k_c$, the transducer gain G_T decreases for the primary resonance. For coupling coefficients larger than the bifurcation coupling, when $k_{01} + k_{02} > k_b$, we observe a nearly constant G_T for variable coupling when using the secondary resonances. Note that this nearly constant G_T at the secondary resonances is significantly larger compared to the G_T at the main resonance.

B. EXPERIMENTAL VALIDATION

An experimental setup using one transmitter and two receivers, operating at a primary resonance frequency of 1 MHz, has been realized to validate the coupling-independent power transfer and efficiency regime observed in the theoretical results, as illustrated in Fig. 6. The sinusoidal current source to drive the circuit is realized using a class-E inverter. Printed circuit boards are used to form the capacitive link. The transmitter plate dimensions are set at 300 mm × 300 mm, while the receiver plates measure 145 mm × 300 mm. The manipulation of the coupling coefficient is achieved by adjusting the distance between the plates. Parallel compensation circuits are applied on the primary and secondary sides, using the circuit parameters as listed in Table 2. Two distinct systems (system 1 and system 2) are used, which feature

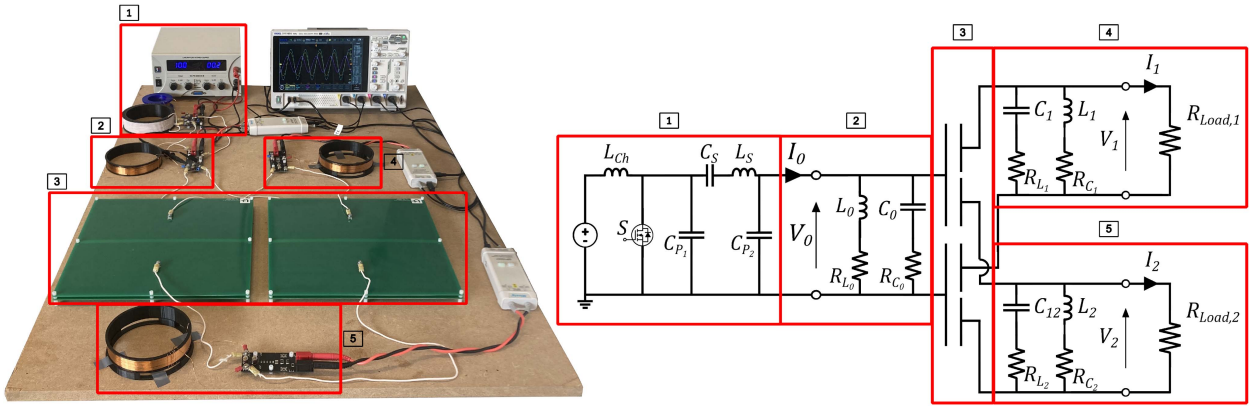

FIGURE 6. Low power (up to 5 W) measurement setup used for experimental validation and schematic overview of the equivalent circuit with (1) a DC power supply and class-E inverter, (2) the primary parallel compensation circuit, (3) the capacitive link interface, and (4,5) the two secondary compensation circuits with the load resistances $R_{Load,1}$ and $R_{Load,2}$.

TABLE 2. Values of Experimental Setup Components

Parameter	Value		Unit
L_0	158.7		µH
L_1	170.1		µH
L_2	170.5		µH
R_{L_0}	4.580		Ω
R_{L_1}	4.920		Ω
R_{L_2}	4.390		Ω
R_{C_0}	6.120		Ω
R_{C_1}	6.240		Ω
R_{C_2}	6.844		Ω
	System 1	**System 2**	
$R_{Load,1}$	9.96	19.98	kΩ
$R_{Load,2}$	9.98	19.92	kΩ

TABLE 3. Coupling Coefficients for Different Distances Between the Plates

Distance [mm]	Coupling coefficient k [-]
5	0.1879
6	0.1645
7	0.1470
8	0.1386
10	0.1155
12	0.1021
17	0.0778
20	0.0685
30	0.0473
40	0.0371

different load resistances $R_{Load,1}$ and $R_{Load,2}$. Note that the values of these systems correspond to a normalized system with $r_{L_0} = r_{L_1} = 0.0046$, $r_{L_2} = 0.0041$, $r_{C_0} = 0.0061$, $r_{C_1} = 0.0058$, $r_{C_2} = 0.0064$, with $g_{L,1} = g_{L,2} = 0.1073$ for system 1 and $g_{L,1} = 0.0535$, $g_{L,2} = 0.0536$ for system 2.

The total capacitance, which is equal to the sum of the individual coupling capacitances, is measured according to the methodology in [31]. Assuming the individual coupling capacitances C_{01} and C_{02} to be equal due to the symmetry of the system, the coupling capacitances can be calculated using the main coupling capacitance C_M, cross coupling capacitance C_C and leakage capacitance C_L:

$$C_{01} = C_{02} = \frac{1}{2}\frac{C_M^2 - C_C^2}{C_M + C_C}. \tag{43}$$

With the obtained coupling capacitances, the coupling coefficient k ($k \approx k_{01} \approx k_{02}$) is calculated using (12). The obtained coupling coefficients for each distance between the plates are shown in Table 3.

To tune the circuit at a resonant frequency of 1 MHz at different plate distances, a trimmer capacitor is incorporated. In order to tune the system, the following procedure is used:

A voltage source is connected at the primary side and the trimmer capacitors at the secondary sides are tuned such that the voltage over each load resistance reach a 90-degree phase shift with the voltage source. Then, a resistor is connected in series with the voltage source, and the trimmer capacitor at the primary side is tuned such that the input voltage and current are in phase.

The secondary resonances $u_\pm$ are then found by increasing and decreasing the frequency from the primary resonance frequency ($u = 1$), until the voltage and current are in phase and hence, the input admittance is purely real.

Figs. 7 and 8 demonstrate a close correspondence between the simulated and measured primary ($u = 1$) and secondary resonance frequencies $u_\pm$ as a function of the coupling coefficient k. From Fig. 7 it is evident that for system 1, the frequency bifurcation occurs around a coupling coefficient k equal to 0.082. At lower coupling values, only the primary resonance frequency ($u = 1$) is present, whereas for higher coupling values, the secondary resonance frequencies $u_\pm$ emerge alongside the primary resonance frequency ($u = 1$). Fig. 8 shows a similar behavior for system 2, however, for this system the bifurcation already occurs around a coupling coefficient k equal to 0.044.

The experimental waveforms are shown in Fig. 9. The input power P_{in} is calculated by averaging the product of input

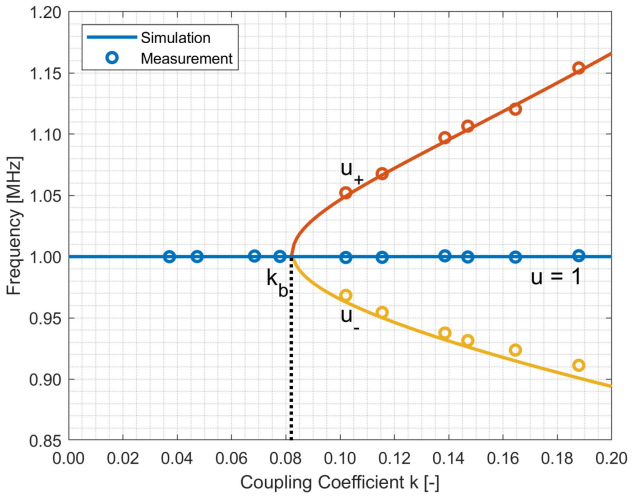

FIGURE 7. Simulated and measured primary ($u = 1$) and secondary $u_\pm$ resonance frequencies as a function of the coupling coefficient $k \approx k_{01} \approx k_{02}$ for system 1, with output resistances $R_{Load,1}$ and $R_{Load,2}$ equal to 10 kΩ, showing the frequency bifurcation for coupling coefficients higher than the bifurcation coupling k_b.

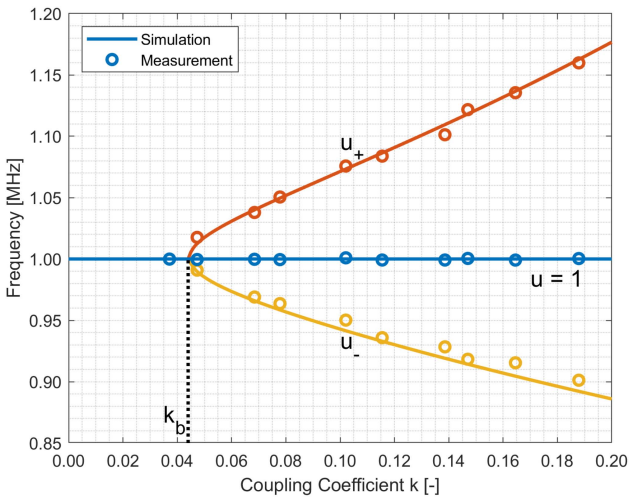

FIGURE 8. Simulated and measured primary ($u = 1$) and secondary $u_\pm$ resonance frequencies as a function of the coupling coefficient $k \approx k_{01} \approx k_{02}$ for system 2, with output resistances $R_{Load,1}$ and $R_{Load,2}$ equal to 20 kΩ, showing the frequency bifurcation.

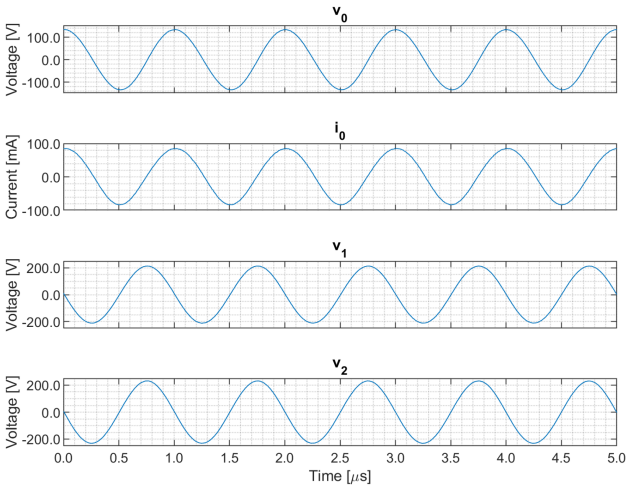

FIGURE 9. Experimental waveforms of the input voltage v_0, input current i_0 and output voltages v_1 and v_2 as captured by the oscilloscope for system 1 at a plate distance of 5 mm.

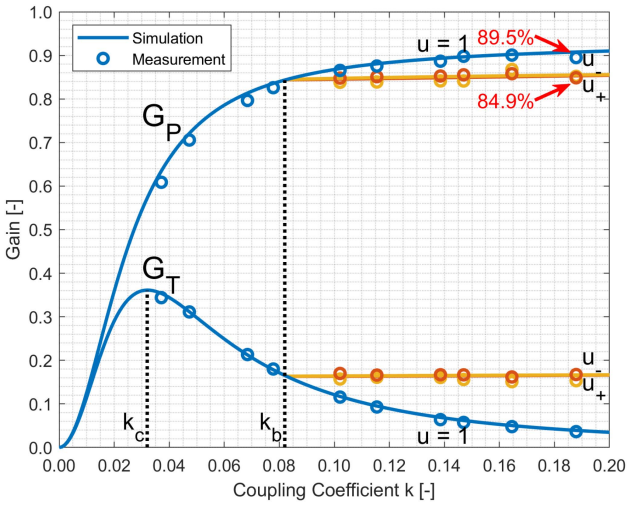

FIGURE 10. Simulated and measured power gain G_P and transducer gain G_T as a function of the coupling coefficient $k \approx k_{01} \approx k_{02}$ for system 1, with output resistances $R_{Load,1}$ and $R_{Load,2}$ equal to 10 kΩ, showing a (nearly) constant efficiency and power output for the secondary resonant frequencies.

voltage v_0 and input current i_0. The output power P_{out} is determined by averaging the squared output voltages v_1 and v_2 divided by the corresponding output resistor. The efficiency, or power gain G_P is then given by:

$$G_P = \frac{P_{out}}{P_{in}}. \tag{44}$$

The simulated and measured power gain G_P and transducer gain G_T as a function of the coupling coefficient k for system 1, shown in Fig. 10, clearly shows the nearly constant efficiency and output power for coupling coefficients higher than the bifurcation coupling coefficient, which is in accordance with the theoretical results. For the given system, the bifurcation occurs at a coupling coefficient k equal to 0.082, and the power gain G_P and transducer gain G_T are slightly higher for the lower secondary resonant frequency u_-. For the highest measured coupling coefficient k of 0.1879, we can see a more than four-fold increase of the transducer gain G_T at the cost of less than 5 % absolute efficiency.

The simulated and measured power gain G_P and transducer gain G_T as a function of the coupling coefficient for system 2 are shown in Fig. 11. Similarly as for system 1, the nearly constant efficiency and output power can be observed for the secondary resonance frequencies $u_\pm$, however for this system the bifurcation already occurs at a coupling coefficient k equal to 0.044, and the difference in power gain G_P and transducer gain G_T between the primary ($u = 1$) and secondary resonances $u_\pm$ is larger. Hence, the increase in transducer gain G_T for the secondary resonances is larger

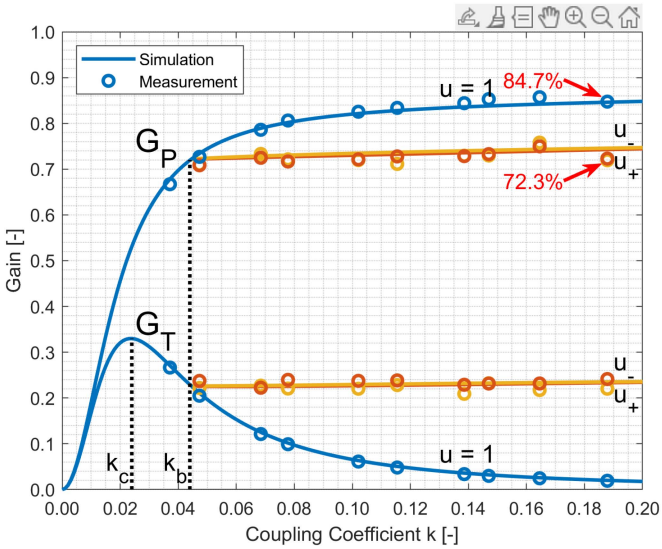

FIGURE 11. Simulated and measured power gain G_P and transducer gain G_T as a function of the coupling coefficient $k \approx k_{01} \approx k_{02}$ for system 2, with output resistances $R_{Load,1}$ and $R_{Load,2}$ equal to 20 kΩ, showing a (nearly) constant efficiency and power output for the secondary resonant frequencies.

(more than eleven-fold increase) but comes at a higher cost in terms of absolute efficiency (a drop of more than 12 %).

The power gain and transducer gain of the system as analyzed in this paper does not consider losses incurred in power converters and additional compensation schemes which are present in practical implementations. While we present the gains solely within the parallel LC compensated capacitive links, it is important to acknowledge that practical applications will introduce extra losses through power electronics and additional compensation schemes, which will lead to lower gains.

Regarding the behavior of the system with power converters, our theoretical framework assumes a current source configuration. In practical WPT configurations, the LCLC configuration is frequently employed [32], [33], [34]. This configuration of the compensation scheme acts approximately as an independent current source [35]. Consequently, the assumption of a current source in our theoretical framework holds in practical systems.

The distribution of power within the proposed SIMO CPT system depends on the coupling coefficient. However, it is worth noting that scenarios where power requirements vary among receivers require a different approach to power division. Although this falls outside the scope of this study, it is an important aspect for future investigations. We refer to [36], [37], [38] for an overview of different power dividing techniques in WPT applications.

Expanding the number of receivers in CPT systems with multiple receivers inevitably leads to a larger electrode area. While this expansion may present practical challenges, such as increased complexity and potential space constraints, its implications must be carefully assessed within the specific context of the application at hand. Indeed, the advantages of a larger electrode area may outweigh any drawbacks in certain scenarios, highlighting the importance of tailored design considerations.

The theoretical framework developed for SIMO systems can also be applied to multiple input, single output systems (MISO), due to the duality between primary and secondary sides in CPT systems [39]. This opens the door for additional research into MISO configurations, allowing us to explore the potential benefits and challenges of this approach in practical applications.

IV. CONCLUSION

We analytically determined expressions for the power gain G_P and transducer gain G_T for SIMO CPT systems, and showed that these are nearly coupling-independent for the secondary resonances $u_{\pm}$, resulting in a nearly constant efficiency and power output despite varying coupling. An experimental setup with one transmitter and two receivers was realized to validate the analytical results.

The theoretical results are shown using an illustrative numerical example. The presented results clearly show the advantage in terms of power transfer to the load for coupling-independent modes. This advantage shown in the theoretical results is confirmed by measurements performed on an experimental setup for two distinct system configurations.

Our findings align with prior research, such as [14], where frequency bifurcation enhanced coupling-independent power output and efficiency for SISO IPT systems, and [23], where similar benefits were observed for SISO CPT systems. We have demonstrated the effectiveness of using frequency bifurcation to achieve coupling-independent power output and efficiency in SIMO CPT systems. Noteworthy is our extension beyond existing literature by incorporating experimental validation, providing empirical validation to the derived expressions for power gain G_P and transducer gain G_T.

This work has showed that accepting a slight decrease in efficiency allows for coupling-independent SIMO CPT system designs with increased power transfer to the load. Two realizations of coupling-independent SIMO CPT systems are presented, the first system showing a four-fold increase in power transfer at the cost of less than 5 % absolute efficiency and the second system showing a eleven-fold increase at the cost of 12 % absolute efficiency.

For future research, the findings from this study can be used for the implementation of frequency-agile control optimization algorithms. Exploring the integration of these results into such an algorithm could provide valuable insights into enhancing the performance and adaptability of SIMO CPT systems across varying conditions.

REFERENCES

[1] J. Kim and F. Bien, "Electric field coupling technique of wireless power transfer for electric vehicles," in *Proc. IEEE Tencon - Spring*, 2013, pp. 267–271, doi: 10.1109/TENCONSpring.2013.6584453.

[2] F. Lu, H. Zhang, and C. Mi, "A review on the recent development of capacitive wireless power transfer technology," *Energies*, vol. 10, 2017, Art. no. 1752, doi: 10.3390/en10111752.

[3] M. Z. Erel, K. C. Bayindir, M. T. Aydemir, S. K. Chaudhary, and J. M. Guerrero, "A comprehensive review on wireless capacitive power transfer technology: Fundamentals and applications," *IEEE Access*, vol. 10, pp. 3116–3143, 2022, doi: 10.1109/ACCESS.2021.3139761.

[4] A. P. Hu, C. Liu, and H. L. Li, "A novel contactless battery charging system for soccer playing robot," in *Proc. IEEE 15th Int. Conf. Mechatron. Mach. Vis. Pract.*, 2008, pp. 646–650, doi: 10.1109/MMVIP.2008.4749606.

[5] J. Dean, M. Coultis, and C. V. Neste, "Wireless sensor node powered by unipolar resonant capacitive power transfer," in *Proc. IEEE PELS Workshop Emerg. Technol.: Wireless Power Transfer*, 2021, pp. 1–5, doi: 10.1109/WoW51332.2021.9462877.

[6] M. R. Coultis, J. Dean, C. Murray, and C. W. V. Neste, "Capacitive powered sensor network using a series transmission line," in *Proc. IEEE PELS Workshop Emerg. Technol.: Wireless Power Transfer*, 2020, pp. 84–87, doi: 10.1109/WoW47795.2020.9291255.

[7] C. Zhang, R. Gallichan, D. M. Budgett, and D. McCormick, "A capacitive pressure sensor interface IC with wireless power and data transfer," *Micromachines*, vol. 11, 2020, Art. no. 897, doi: 10.3390/mi11100897.

[8] H. A. Fadhil, S. G. Abdulqader, and S. A. Aljunid, "Implementation of wireless power transfer system for smart home applications," in *Proc. IEEE 8th GCC Conf. Exhib.*, 2015, pp. 1–4, doi: 10.1109/IEEEGCC.2015.7060042.

[9] J. V. Mulders et al., "Wireless power transfer: Systems, circuits, standards, and use cases," *Sensors*, vol. 22, 2022, Art. no. 5573, doi: 10.3390/s22155573.

[10] V.-B. Vu et al., "A multi-output capacitive charger for electric vehicles," in *Proc. IEEE 26th Int. Symp. Ind. Electron.*, 2017, pp. 565–569, doi: 10.1109/ISIE.2017.8001308.

[11] M. Dionigi, M. Mongiardo, and R. Perfetti, "Rigorous network and full-wave electromagnetic modeling of wireless power transfer links," *IEEE Trans. Microw. Theory Techn.*, vol. 63, no. 1, pp. 65–75, Jan. 2015, doi: 10.1109/TMTT.2014.2376555.

[12] M. Dionigi, M. Mongiardo, G. Monti, and R. Perfetti, "Modelling of wireless power transfer links based on capacitive coupling," *Int. J. Numer. Modelling: Electron. Netw., Devices Fields*, vol. 30, 2017, Art. no. e2187, doi: 10.1002/jnm.2187.

[13] B. Minnaert, M. Mongiardo, A. Costanzo, and F. Mastri, "Maximum efficiency solution for capacitive wireless power transfer with N receivers," *Wireless Power Transfer*, vol. 7, no. 1, pp. 65–75, 2020, doi: 10.1017/wpt.2020.9.

[14] F. Mastri, A. Costanzo, and M. Mongiardo, "Coupling-independent wireless power transfer," *IEEE Microw. Wireless Compon. Lett.*, vol. 26, no. 3, pp. 222–224, Mar. 2016, doi: 10.1109/LMWC.2016.2524560.

[15] C. S. Wang, G. A. Covic, and O. H. Stielau, "Power transfer capability and bifurcation phenomena of loosely coupled inductive power transfer systems," *IEEE Trans. Ind. Electron.*, vol. 51, no. 1, pp. 148–157, Feb. 2004, doi: 10.1109/TIE.2003.822038.

[16] J.-W. Lee, D.-G. Woo, S.-H. Ryu, B.-K. Lee, and H.-J. Kim, "Practical bifurcation criteria considering coil losses and compensation topologies in inductive power transfer systems," in *Proc. IEEE Int. Telecommun. Energy Conf.*, 2015, pp. 1–6, doi: 10.1109/INTLEC.2015.7572435.

[17] I. Karakitsios and N. Hatziargyriou, "Bifurcation in dynamic inductive charging of electric vehicles," in *Proc. IEEE Manchester PowerTech*, 2017, pp. 1–6, doi: 10.1109/PTC.2017.7981055.

[18] M. Kosik and J. Lettl, "Analysis of bifurcation in series-series and series-parallel compensated inductive power transfer," in *Proc. IEEE PELS Workshop Emerg. Technol.: Wireless Power Transfer*, 2019, pp. 75–80, doi: 10.1109/WoW45936.2019.9030605.

[19] A. D. Scher and M. Kosik, "Novel method of metal object detection based on the bifurcation phenomena in inductive power transfer," in *Proc. Wireless Power Week*, 2022, pp. 567–571, doi: 10.1109/WPW54272.2022.9853970.

[20] Y. Zhang, Z. Zhao, and K. Chen, "Frequency-splitting analysis of four-coil resonant wireless power transfer," *IEEE Trans. Ind. Appl.*, vol. 50, no. 4, pp. 2436–2445, Jul./Aug. 2014, doi: 10.1109/TIA.2013.2295007.

[21] M. Iordache, L. Mandache, D. Niculae, and L. Iordache, "On exact circuit analysis of frequency splitting and bifurcation phenomena in wireless power transfer systems," in *Proc. Int. Symp. Signals, Circuits Syst.*, 2015, pp. 1–4, doi: 10.1109/ISSCS.2015.7203929.

[22] H. Nguyen and J. I. Agbinya, "Splitting frequency diversity in wireless power transmission," *IEEE Trans. Power Electron.*, vol. 30, no. 11, pp. 6088–6096, Nov. 2015, doi: 10.1109/TPEL.2015.2424312.

[23] B. Minnaert, F. Mastri, N. Stevens, A. Costanzo, and M. Mongiardo, "Coupling-independent capacitive wireless power transfer using frequency bifurcation," *Energies*, vol. 11, 2018, Art. no. 1912, doi: 10.3390/en11071912.

[24] D.-W. Seo and J.-H. Lee, "Frequency-tuning method using the reflection coefficient in a wireless power transfer system," *IEEE Microw. Wireless Compon. Lett.*, vol. 27, no. 11, pp. 959–961, Nov. 2017, doi: 10.1109/LMWC.2017.2750023.

[25] W. Gu, D. Qiu, X. Shu, B. Zhang, W. Xiao, and Y. Chen, "A constant output capacitive wireless power transfer system based on parity-time symmetric," *IEEE Trans. Circuits Syst. II: Exp. Briefs*, vol. 70, no. 7, pp. 2585–2589, Jul. 2023, doi: 10.1109/TCSII.2023.3237687.

[26] M. B. Lillholm, Y. Dou, X. Chen, and Z. Zhang, "Analysis and design of 10-MHz capacitive power transfer with multiple independent outputs for low-power portable devices," *IEEE Trans. Emerg. Sel. Topics Power Electron.*, vol. 10, no. 1, pp. 149–159, Feb. 2022, doi: 10.1109/JESTPE.2020.3035493.

[27] C. Lecluyse, M. Kleemann, and B. Minnaert, "Frequency bifurcation conditions for capacitive wireless power transfer with multiple receivers," in *Proc. Wireless Power Week*, 2022, pp. 807–811, doi: 10.1109/WPW54272.2022.9901346.

[28] A. v. Ieperen, S. Derammelaere, and B. Minnaert, "Coupling-independent capacitive wireless power transfer with one transmitter and two receivers using frequency bifurcation," in *Proc. IEEE-APS Topical Conf. Antennas Propag. Wireless Commun.*, 2023, pp. 042–047, doi: 10.1109/APWC57320.2023.10297497.

[29] B. Minnaert, G. Monti, A. Costanzo, and M. Mongiardo, "Power maximization for a multiport network described by the admittance matrix," *URSI Radio Sci. Lett.*, vol. 2, pp. 1–5, 2021, doi: 10.46620/20-0029.

[30] J. C. Sten and M. Hirvonen, "Impedance and quality factor of mutually coupled multiport antennas," *Microw. Opt. Technol. Lett.*, vol. 50, pp. 2034–2039, Aug. 2008, doi: 10.1002/mop.23564.

[31] L. Huang and A. P. Hu, "Defining the mutual coupling of capacitive power transfer for wireless power transfer," *Electron. Lett.*, vol. 51, pp. 1806–1807, Oct. 2015, doi: 10.1049/el.2015.2709.

[32] F. Lu, H. Zhang, H. Hofmann, and C. Mi, "A double-sided LCLC-compensated capacitive power transfer system for electric vehicle charging," *IEEE Trans. Power Electron.*, vol. 30, no. 11, pp. 6011–6014, Nov. 2015, doi: 10.1109/TPEL.2015.2446891.

[33] F. Lu, H. Zhang, H. Hofmann, and C. C. Mi, "A double-sided LC-compensation circuit for loosely coupled capacitive power transfer," *IEEE Trans. Power Electron.*, vol. 33, no. 2, pp. 1633–1643, Feb. 2018, doi: 10.1109/TPEL.2017.2674688.

[34] D. B. Cobaleda, C. Suarez, and W. Martinez, "Input impedance analysis of an LCLC type capacitive power transfer converter," in *Proc. 23rd Eur. Conf. Power Electron. Appl.*, 2021, pp. P.1–P.9, doi: 10.23919/EPE21ECCEEurope50061.2021.9570575.

[35] A. Reatti, S. Musumeci, and F. Corti, "Frequency analysis and comparison of LCCL and CLLC compensations for capacitive wireless power transfer," in *Proc. AEIT Int. Conf. Elect. Electron. Technol. Automot.*, 2020, pp. 1–6, doi: 10.23919/AEITAUTOMOTIVE50086.2020.9307429.

[36] Y. Zhang, T. Lu, Z. Zhao, F. He, K. Chen, and L. Yuan, "Selective wireless power transfer to multiple loads using receivers of different resonant frequencies," *IEEE Trans. Power Electron.*, vol. 30, no. 11, pp. 6001–6005, Nov. 2015, doi: 10.1109/TPEL.2014.2347966.

[37] W. Liu, K. T. Chau, C. H. T. Lee, C. Jiang, W. Han, and W. H. Lam, "Multi-frequency multi-power one-to-many wireless power transfer system," *IEEE Trans. Magn.*, vol. 55, no. 7, Jul. 2019, Art no. 8001609, doi: 10.1109/TMAG.2019.2896468.

[38] W. Lee, W. Lee, and D. Ahn, "Maximum efficiency conditions satisfying power regulation constraints in multiple-receivers wireless power transfer," *Energies*, vol. 15, no. 10, 2022, Art. no. 3840, doi: 10.3390/en15103840.

[39] B. Minnaert, A. Costanzo, G. Monti, and M. Mongiardo, "Capacitive wireless power transfer with multiple transmitters: Efficiency optimization," *Energies*, vol. 13, no. 13, 2020, Art. no. 3482, doi: 10.3390/en13133482.

ARIS VAN IEPEREN (Student Member, IEEE) received the B.Sc. degree in mechanical engineering and the M.Sc. degree in systems & control from the Eindhoven University of Technology, Eindhoven, The Netherlands, in 2019 and 2022 respectively. He was a Junior Researcher with University Medical Center Utrecht, Utrecht, The Netherlands. He is currently working toward the Ph.D. degree in capacitive wireless power transfer for MIMO configurations with the University of Antwerp, Antwerp, Belgium. His research interests include power electronics, wireless power tansfer and control systems.

STIJN DERAMMELAERE (Member, IEEE) was born in Kortrijk, Belgium, in 1984. He received the M.Sc. degree in automation from the Technical University College of West-Flanders, Kortrijk, in 2006, and the Ph.D. degree in 2013 from Ghent University, Ghent, Belgium, where he initiated research concerning control engineering, co-design of control and mechatronic systems and the motion control of fractional horsepower machines. He continues this research since 2017 with the University of Antwerp, Antwerp, Belgium, where he has been an Associate Professor in mechatronics since 2022. In 2023 he also became a guest-Professor with the Lappeenranta University of Technology, Lappeenranta, Finland. He teaches control engineering and motion optimization at the Faculty of Applied Engineering. Dr. Derammelaere coordinated more than ten projects till 2022 and is the co-author of 57 articles included in de Web of Science. His expertise includes co-design, motion control and optimization of mechatronic systems. He is an Associate Editor for *Discover Mechanical Engineering* Springer journal.

BEN MINNAERT (Member, IEEE) received the M.Sc. degree in engineering physics and the Ph.D. degree in modeling of photovoltaic solar cells from Ghent University, Ghent, Belgium, in 2003 and 2007, respectively. He is currently an Assistant Professor with the University of Antwerp, Antwerp, Belgium and focuses his research on energy modeling. His research interest include wireless power transfer, electromagnetism and circuit theory.